Spurs-Free Single-Bit-Output All-Digital Frequency Synthesizers With Forward and Feedback Spurs and Noise Cancellation

Paul P. Sotiriadis, *Senior Member, IEEE*

***Abstract*—All-digital frequency synthesis architectures with phase and polar Σ–Δ modulation feedback loops are introduced as a means to overcome the inherent spectral-quality limitations of forward-dithered all-digital frequency synthesizers represented by the family of pulse direct digital synthesizers. The spectrum of dithered pulse direct digital synthesizers is derived first, with and without modulation, as well as that of their variations with multiple dithered paths and with colored dithering resulting in lower noise level. The limited dynamic range achieved by forward-dithered all-digital frequency synthesizers motivates the introduction of phase and polar Σ–Δ modulation feedback loop architectures which are modeled and analyzed to derive their noise transfer functions. Extensive MATLAB simulation illustrates the suppressed near-in noise and the high spurs-free dynamic range the two Σ–Δ schemes can achieve and the wideband spurs-free output of the polar one. Detailed analysis and implementation aspects of the techniques are outside the scope of the paper.**

***Index Terms*—Digital signal processing, digital-to-analog converter, digital-to-frequency converter, direct digital synthesis, feedback loop, filter, frequency spurs, noise shaping, quantization, spectrum, stability.**

I. Introduction

THERE are at least two reasons making direct all-digital frequency synthesizers with single-bit output attractive. The first is the convenience of digital circuits in terms of design and operation, especially for VLSI implementation. The powerful automation tools for design, verification and layout of digital circuits and the convenience of almost automated migration of existing ones to future technology nodes offer a tremendous advantage over analog and mixed-signal alternatives whose design or migration becomes more and more challenging with technology downscaling. In addition, all-digital frequency synthesizers may take less chip area, they are easier to co-integrate with DSP blocks and are more noise and PVT variation tolerant than their analog counterparts.

A second noteworthy advantage of single-bit output all-digital frequency synthesizers is their potential to achieve higher dynamic range (DR) as well as spurious free dynamic range (SFDR) near-in in comparison to the classical direct digital synthesizes (DDS) [1]. The reason is that although standard DDS (Fig. 1) can have very high DR and SFDR in the digital domain, the conversion to the analog domain with a multi-bit DAC degrades the spectral quality [2]. The DAC's limited number of effective bits (ENOB) (small for high sampling rates) and its nonlinearity in general are major sources of spurs and noise in DDS and constitute the dominant limiting factors in DDS' SFDR and DR. In addition, high speed DACs are challenging to design and are very power hungry. In contrast to classical DDS, all-digital frequency synthesizers with single-bit output have a serial 0/1 binary output which is easier to convert to the analog domain. With only two levels, the possible conversion errors in a carefully designed circuit are the amplitude and the offset, both of which are negligible for most applications, compared to those of a fast multi-bit DAC.

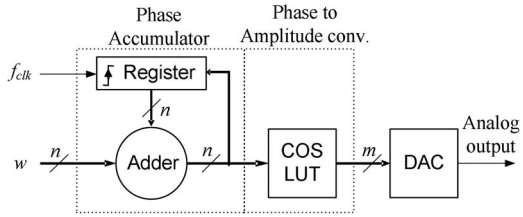

Fig. 1. Basic form of DDS.

This paper reviews recent all-digital frequency synthesis techniques with *forward* dithering for spurs elimination and introduces two new *feedback* architectures capable of achieving high SFDR and DR near-in. The approach is from an abstract point of view and it is constrained to the presentation of a brief mathematical analysis and a qualitative illustration of the concepts. Detailed analysis and hardware implementation aspects are outside of this paper's scope.

Specifically, Section II discusses the concept of pulse-DDS and its equivalence to single-bit sinewave quantization illustrating the constraints of it in generating a spectrally clean single-bit output. This motivates the use of dithering. A brief derivation of the generated spectrum using dithering with and without amplitude modulation is provided. The derived noise floor level indicates the need for noise shaping/reduction techniques. The use of parallel quantization paths for noise reduction is presented and analyzed, and the use of colored dithering is discussed briefly.

Manuscript received October 18, 2015; revised December 19, 2015; accepted January 28, 2016. Date of current version June 28, 2016. This work was partially supported by Broadcom Foundation USA. This paper was recommended by Associate Editor E. A. Barros da Silva.

The author is with National Technical University of Athens, Greece (e-mail: pps@ieee.org).

Color versions of one or more of the figures in this paper are available online at http://ieeexplore.ieee.org.

Digital Object Identifier 10.1109/TCSI.2016.2525058

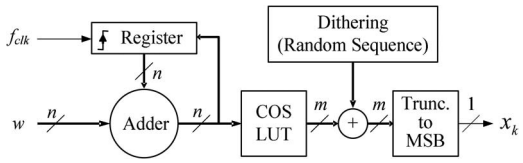

Fig. 2. PDDS with amplitude random dithering.

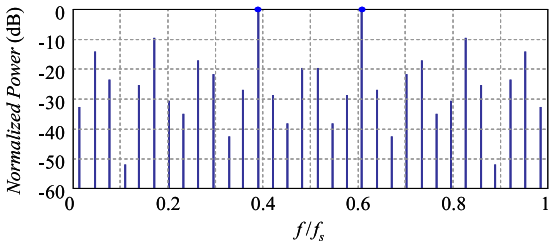

Fig. 3. Spectrum of undithered PDDS with $w = 25$ and $n = 6$. See footnote1.

Section III introduces the *phase* and the *polar* Σ–Δ modulation—all-digital frequency synthesis architectures. The first one uses simple phase-error estimation of the quantized output and feedback. A brief mathematical analysis is presented based on simplifying assumptions to extract a small-signal model and derive the noise transfer function from the dither source to the output. MATLAB simulation illustrates the capabilities of the architecture. Addition of amplitude feedback results in the *Polar* Σ–Δ modulation scheme which implements amplitude control by controlling the power (standard deviation) of the dithering sequence. A brief mathematical analysis of this highly nonlinear two-coupled loop scheme provides insight of its operation. MATLAB simulation illustrates the capabilities of high near-in SFDR and DR and wideband spurs-free output of the architecture.

II. Forward Architectures

Efforts to develop fully-digital frequency synthesizers offering all advantages of digital circuits date at least three decades back [3]–[5]. A way to get such architectures is to remove the DAC in DDS (Fig. 1), i.e., the only analog/mixed-signal block in standard DDS, and use for example the MSB of the LUT as the output (see footnote[1]). This leads to the finite state machine (FSM) with single-bit (SB) output in Fig. 2, often called pulse-DDS (PDDS). This direct all-digital synthesizer that does not have an oscillator (in contrast to all-digital PLL [6], [7]) has the inherent challenge of generating a single-bit digital output with the desirable sinewave-like spectrum using only timing of the reference clock [3], [8].

With the exception of generating an output frequency equal to an integer fraction of the clock, the output waveform is irregular with high deterministic jitter and a spectrum full of strong spurs which can be very close to the carrier, as shown in Fig. 3. This general problem of FSM type architectures with SB output demands the use of additional techniques for suppressing the strong spurious signals. Several such techniques have been proposed [8] with random dithering being the only purely digital one.

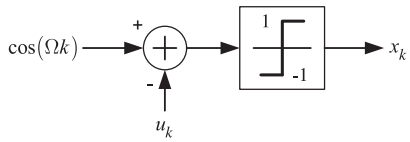

Fig. 4. Dithered single-bit-quantized sinewave imitating PDDS.

The problem of generating spurious-free output with a dithered PDDS has been studied in abstract form in [9]. It is shown that random dithering having appropriate statistics results in spurs-free output [9]–[11]. However, in some sense, dithering converts the frequency spurs into a noise floor.

A. Eliminating Spurs With Dithering

Consider the DDS and the PDDS schemes in Figs. 1 and 2 respectively. The finite resolution of the LUT's output introduces a representation error of the cosine function in the order of $-6m$ dBc [12]. This error is negligible compared to that introduced by the crude single-bit (MSB) quantization at the output in Fig. 2. This motivates the abstract model in Fig. 4, which is approximately equivalent to that in Fig. 2 and whose accuracy improves with m.

The phase of the cosine in Fig. 4 is Ωk, where $k \in \mathbb{Z}$ is the discrete time index and Ω is the discrete-time frequency.

Using an n-Bit phase accumulator $\Omega = 2\pi w/2^n$, where $0 < w < 2^{n-1}$ is the *frequency control word*. The accumulator's value is $\mathrm{Ph}_k = (\mathrm{kw}) \bmod 2^n$ and the LUT implements the function $\cos(2\pi \mathrm{Ph}_k/2^n) = \cos(\Omega k)$. The quantization in Fig. 2 is practically equivalent to applying the signum function, as in Fig. 4, i.e.,

$$x_k = \mathrm{sgn}\left(\cos(\Omega k) - u_k\right) \tag{1}$$

which can be expressed as

$$x_k = \begin{cases} 1 & \text{if } u_k < \cos(\Omega k) \\ -1 & \text{if } u_k > \cos(\Omega k) \\ 0 & \text{otherwise.} \end{cases} \tag{2}$$

Also, since the desirable output is $\cos(\Omega k)$ we define the error $e_k \stackrel{\wedge}{=} x_k - \cos(\Omega k)$ and so

$$x_k = \cos(\Omega k) + e_k. \tag{3}$$

The dithering sequence $\{u_k\}$ in Fig. 4 is assumed random. It is interesting however to consider first the case without dithering, i.e., when $u_k = 0$ for all k. Then, with the exception of values of w which are powers of 2, the spectrum of x_k is full of spurs. Specifically the spurs are at frequencies[1] $\omega_\ell = \Omega + 2\pi\ell \cdot \gcd(2w, 2^n)/2^n$, $\ell \in \mathbb{Z}$. Fig. 3 shows the output spectrum for $w = 25$ and $n = 6$.

Now, if $\{u_k\}$ is a random sequence, the output x_k is also random but *not* wide-sense stationary. To define the spectrum

[1]I.e., the spectrum of $x_k = ((\mathrm{kw} + x_0) \bmod 2^n)\mathrm{div}2^{n-1}$ which is a meaningful PDDS implementation. x_0 is the initial state of the accumulator.

of $\{x_k\}$ we derive the time-average autocorrelation (TAA) function of it, [13]

$$\bar{r}_x(k) = \lim_{M\to\infty} \frac{1}{2M+1} \sum_{m=-M}^{M} E\{x_{k+m}x_m\} \tag{4}$$

and take the discrete-time Fourier transform (DTFT) of it

$$s_x(\omega) = \sum_{k=-\infty}^{\infty} \bar{r}_x(k) e^{-jk\omega}. \tag{5}$$

The TAA and spectrum definitions are applied similarly to all random and deterministic sequences we encounter [13].

From here on we assume that the dithering sequence $\{u_k\}$ is formed of random variables which are independent and uniformly distributed (IUD) in $[-1, 1]$. We discuss some simple facts which we use later in our derivations. Let us consider Fig. 4 and for convenience define $v_k = \cos(\Omega k)$ which takes values in $[-1, 1]$ for every Ω and k. From $x_k = \operatorname{sgn}(v_k - u_k)$ we have that $x_k \in \{\pm 1\}$ (note that the probability of $x_k = 0$ is zero and is ignored) and that for every $v_k \in [-1, 1]$ it is

$$\begin{aligned} \Pr(x_k = 1) &= \frac{(1+v_k)}{2} \\ \Pr(x_k = -1) &= \frac{(1-v_k)}{2}. \end{aligned} \tag{6}$$

Equation (6) implies $E\{x_k\} = v_k$ and since $x_k = v_k + e_k$ from (3) we get $E\{e_k\} = 0$ as well as $E\{e_k^2\} = 1 - v_k^2$. Since $\{u_k\}$ is a sequence of independent random variables so is the sequence $\{e_k\}$. Therefore we conclude that

$$E\{e_{k+m}e_m\} = \left(1 - v_m^2\right)\delta_k \tag{7}$$

where δ_k is the discrete time Dirac function. Moreover

$$E\{x_{k+m}x_m\} = v_{k+m}v_m + E\{e_{k+m}e_m\}. \tag{8}$$

Calculating the TAA of $\{e_k\}$ we have

$$\begin{aligned} \bar{r}_e(k) &= \lim_{M\to\infty} \frac{1}{2M+1} \sum_{m=-M}^{M} E\{e_{k+m}e_m\} \\ &= \left[\lim_{M\to\infty} \frac{1}{2M+1} \sum_{m=-M}^{M} \left(1 - \cos^2(m\Omega)\right)\right] \cdot \delta_k = \frac{\delta_k}{2}. \end{aligned}$$

Moreover the TAA of the desirable output $\{v_k\}$ is given by

$$\bar{r}_v(k) = \lim_{M\to\infty} \frac{1}{2M+1} \sum_{m=-M}^{M} E\{v_{k+m}v_m\} = \frac{1}{2}\cos(k\Omega).$$

Equation (8) implies $\bar{r}_x = \bar{r}_v + \bar{r}_e$ and the spectral superposition

$$s_x(\omega) = s_v(\omega) + s_e(\omega). \tag{9}$$

Writing the discrete-time angular frequency as $\omega = 2\pi f/f_s$, where f_s is the sampling (clock) frequency, it can be shown

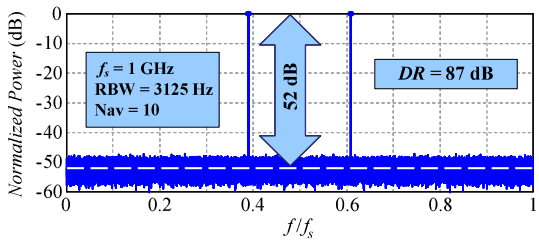

Fig. 5. Output spectrum of PDDS with random variables $\{u_k\}$ being IUD in $[-1, 1]$. Parameter values are $w = 25$ and $n = 6$. Clock frequency is set to $f_s = 1$ GHz, averaging (NAV) is set to 10 frames and resolution bandwidth (RBW) is 3125 Hz.

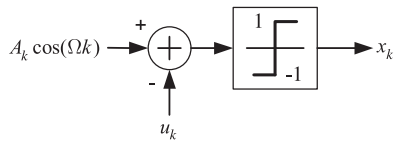

Fig. 6. Uniformly dithered single-bit quantized amplitude-modulated sinewave.

taking the DTFT of $\bar{r}_v$ and $\bar{r}_e$ that

$$s_v\left(\frac{2\pi f}{f_s}\right) = \frac{1}{4}\sum_{k=-\infty}^{\infty} \delta\left(\frac{f}{f_s} \pm \frac{\Omega}{2\pi} - k\right) \tag{10}$$

and $s_e(\omega) = 1/2$, so the error spectrum is flat,[2] Fig. 5 [11].

The output is *spurs-free* and the DR, defined as the ratio of the power of the desirable signal to the power spectral density (PSD) of the near-in noise s_e is $\text{DR} = 10\log_{10}(f_s) - 3.01$ dB, (in the continuous time-domain) [10], [11]. Note that the dynamic range observed in Fig. 5, and in a spectrum analyzer, is $10\log_{10}(\text{RBW})$dB less than the actual DR due to the Resolution Bandwidth (RBW) of the measurement, i.e., in Fig. 5 it is $87 - 10\log_{10}(3125) = 52$.

Amplitude modulation (AM) can be achieved by inserting a digital multiplier immediately after the LUT in Fig. 2. This is modeled in Fig. 6 where $\cos(\Omega k)$ has been replaced by $A_k\cos(\Omega k)$. We set $v_k = A_k\cos(\Omega k)$ for convenience. The previous derivations are valid here as well and (7) is replaced by [10]

$$E\{e_{k+m}e_m\} = \left[1 - E\left\{A_m^2\right\}\cos^2(m\Omega)\right]\delta_k. \tag{11}$$

If A_k is deterministic and as long as $|A_k| \le 1$ and $\{A_k\}$ is band-limited by Ω_A with $0 < \Omega_\text{A} < \Omega < \pi - \Omega_\text{A}$, then $s_x(\omega) = s_v(\omega) + s_e(\omega)$ where s_v is the spectrum of $A_k\cos(\Omega k)$ defined as before [10]. Moreover $s_e(\omega) = 1 - \bar{A}^2/2$, where $\bar{A}^2$ is the average power of $\{A_k\}$. So, the noise floor is flat again and the DR is defined accordingly. Fig. 7 shows the spectrum when $w = 15$, $n = 6$, $A_k = 1/2 + (1/2)\sin(\Omega_\text{mod}\, k)$, $\Omega_\text{mod} = 2\pi \cdot 0.045$, $f_s = 1$ GHz, averaging is on 10 frames, resolution bandwidth is 142 Hz.

When $\{A_k\}$ is a wide-sense stationary random sequence, let $r_A(n) \triangleq E\{A_{n+m}A_m\}$, it is $s_x(\omega) = s_v(\omega) + s_e(\omega)$ as before where $s_v(\omega) = [s_A(\omega - \Omega) + s_A(\omega + \Omega)]/4$ is the

[2]In the discrete-time domain. In the continuous-time domain the shape of the output pulses has to be taken into account as well.

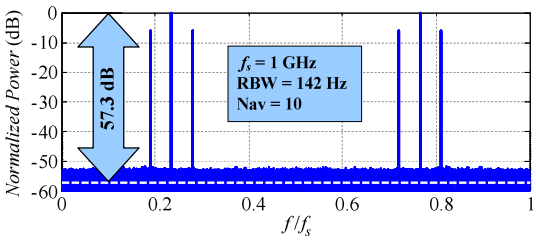

Fig. 7. Output spectrum when $A_k = 1/2 + (1/2)\sin(k\Omega_{\rm mod})$.

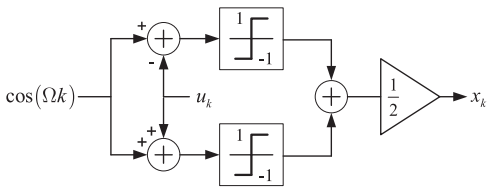

Fig. 8. Averaging the outputs of two PDDS with opposite dithers.

spectrum of $\{A_k \cos(\Omega k)\}$ derived using the TAA. Again the output is spurs-free with $s_e(\omega) = 1 - r_A(0)/2$, [10].

B. Enhancing the Dynamic Range by Parallel Paths

A way to reduce the noise floor introduced by dithering is to use two opposite-dithered quantization paths following the cosine LUT, and add the outputs as shown in Fig. 8. Although the output is not binary, it is differential 0, ± 1. The output 1/2 gain is only for allowing comparison to previous scheme.

The random sequence $\{u_k\}$ is formed of IUD in $[-1,\ 1]$ random variables as before. The output signal is

$$x_k = \frac{1}{2}\Big(\operatorname{sgn}\left(\cos(\Omega k) - u_k\right) + \operatorname{sgn}\left(\cos(\Omega k) + u_k\right)\Big) \quad (12)$$

which *with probability one* is

$$x_k = \begin{cases} \operatorname{sgn}\left(\cos(\Omega k)\right) & \text{if } |u_k| < |\cos(\Omega k)| \\ 0 & \text{otherwise.} \end{cases} \quad (13)$$

Using the derivations of Section II-A and since both random sequences $\{\pm u_k\}$ are uniformly distributed in $[-1,\ 1]$ we have $E\{x_k\} = \cos(\Omega k)$. Moreover since x_{k+m} and x_m are independent, for $k \neq 0$ it is $\bar{r}_x(k) = (1/2)\cos(k\Omega)$. Also, since $\{u_k\}$ is uniformly distributed in $[-1,\ 1]$, (13) gives $\Pr(x_m^2 = 1) = |\cos(m\Omega)|$ for every m. It can be seen that

$$\bar{r}_x(0) = \begin{cases} \dfrac{\sin\left(\frac{2\pi}{2^r}\right)}{2^{r-1}\left[1-\cos\left(\frac{2\pi}{2^r}\right)\right]} & \text{if } r \geq 2 \\ 1 & \text{otherwise} \end{cases}$$

where $r = n - \log_2(\gcd(2^n, w))$, [11]. Combining the above

$$\bar{r}_x(k) = \frac{1}{2}\cos(\Omega k) + \left(\bar{r}_x(0) - \frac{1}{2}\right)\delta_k. \quad (14)$$

Setting the desirable output $v_k = \cos(\Omega k)$ as before we have $\bar{r}_v(k) = \cos(k\Omega)/2$. Extrapolating on the results of the previous section we have $x_k = v_k + e_k$ as well as $\bar{r}_x(k) = \bar{r}_v(k) + \bar{r}_e(k)$ leading to $s_x(\omega) = s_v(\omega) + s_e(\omega)$, [11].

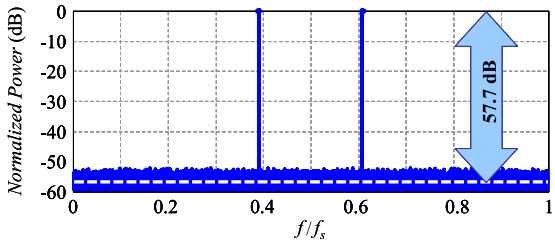

Fig. 9. Spectrum using opposite dithering. Parameter values are $w = 25$ and $n = 6$, clock frequency is $f_s = 1$ GHz, averaging (NAV) is set to 10 frames and Resolution Bandwidth (RBW) is 3125 Hz.

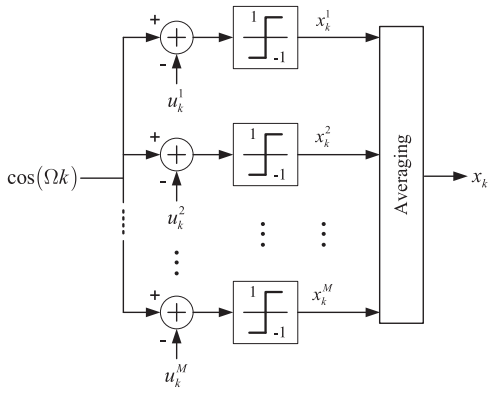

Fig. 10. Multi-path PDDS with parallel independent dithering paths.

Therefore the PSD of the signal is given by Eq. (10), as before, whereas the noise PSD is given by $s_e(\omega) = \bar{r}_x(0) - (1/2)$.

We conclude that when $w \neq 2^{n-2}$ (division by 4) the dynamic range is DR $\cong 10\log_{10}(f_s) + 2.61$ (dB), i.e., about 5.6 dB higher than in the case of Fig. 5, [11]. The corresponding spectrum is shown in Fig. 9 where DR $= 92.6$ dB.

Another similar scheme reducing the noise floor level is shown in Fig. 10. Here M dithering and quantization paths are used with mutually independent random sequences $\{u_k^\ell\}$, $\ell = 1, 2, \ldots, M$, each formed of IUD in $[-1,\ 1]$ random variables. Although it is not a single-bit output scheme, the output averaging is easy to achieve at the circuit or the antenna level.

The output of every individual path $\ell = 1, 2, 3, \ldots, M$ is $x_k^\ell = \operatorname{sgn}(\cos(k\Omega) - u_k^\ell)$ and we can define the corresponding error as before, i.e. $x_k^\ell = \cos(k\Omega) + e_k^\ell$. Then the output is expressed as $x_k = \cos(k\Omega) + (1/M)\sum_{\ell=1}^{M} e_k^\ell$. Since the noise components, e_k^ℓ, $\ell = 1, 2, 3, \ldots, M$ are mutually independent, the output noise power is $1/M$ times that of the simple scheme in Fig. 4. Therefore, the scheme results in dynamic range DR $= 10\log_{10}(f_s) + 10\log_{10}(M) - 3.01$ (dB), demonstrating an improvement of $10\log_{10}(M)$ dB compared to that of the scheme in Fig. 4, [11].

C. Enhancing the Dynamic Range With Colored Dither

Finally, colored uniformly distributed dither instead of white (IUD) one can result in spurs-free output with slightly higher DR, e.g., about 2.5 dB better as shown in Fig. 11 [11].

However, the computational cost of generating appropriately colored and marginally uniformly distributed random dithering

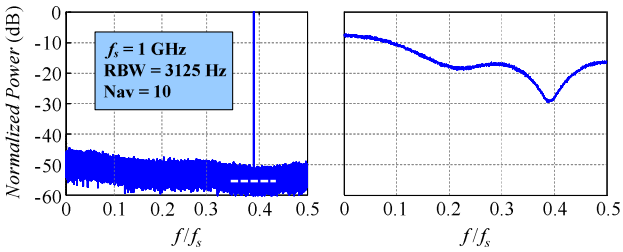

Fig. 11. Colored-dithered PDDS output spectrum (left). Spectrum of the colored, uniformly distributed dither (right).

sequences is in most cases disproportionate to the improvements in the dynamic range [14].

D. Comments on the Forward Architectures

Although dithering in forward architectures may remove spurs it does introduce noise in the form of a noise floor. White uniformly distributed (IUD) dithering results in dynamic range in the order of $10\log_{10}(f_s)$. Colored dithering sequences can improve the dynamic range but not significantly [11]. Other classes of similar synthesizers like Flying-Adder and all-digital period-synthesizers typically suffer from the same output noise floor, when dither is used to eliminate the spurs [15]–[21]. These limitations motivate the use of a feedback mechanism to shape the PSD of the noise away from the carrier. Σ–Δ modulation comes as a natural choice and two new such architectures are introduced in the following section.

III. Feedback (Σ–Δ) Architectures

The inherent disadvantage of the forward dithering techniques for spurs suppression is that the power of dither spreads throughout the whole spectrum raising the noise floor level, as shown in Fig. 5.

The use of colored dither as in Fig. 11 appears to have limited ability in shifting noise power away from the carrier. This is because of the strong nonlinearity of the quantizer's signum function which acts as a signal mixer blending the colored noise spectrum with the carrier signal's harmonic frequencies. To the best of the author's knowledge there is no formal bound on how much colored dither can shape the output noise spectrum to our desire. On the other hand, experience indicates that generating in real time any potentially useful colored dither with appropriate statistics is challenging in terms of computational complexity.

Feedback Σ–Δ architectures instead are very efficient in noise shaping resulting in high DR and ideally spurs-free band of interest in many signal processing architectures [2], [22]–[24]. The concept of Σ–Δ modulation is used here to generate single-bit output synthesizers with sinewave-like and clean near-in spectrum.

Two new classes of such synthesizers are introduced in the following sections, the *Phase-Domain* Σ–Δ *Modulator* and the *Polar* Σ–Δ *Modulator*.

A. Phase-Domain Σ–Δ Modulation

The case of forward dithering in Fig. 4 with IUD dither results in spurs-free output. It can be shown that we get the same spurs-free output spectrum with flat noise floor (discrete-time domain) using the architecture in Fig. 12, [9].

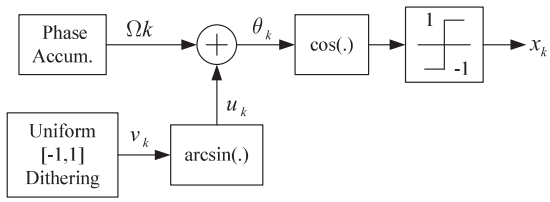

Fig. 12. Phase-dithered synthesizer with spurs-free output.

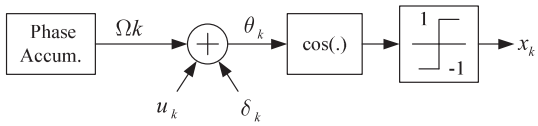

Fig. 13. Phase noise feedback.

The output is $x_k = \mathrm{sgn}(\cos(\Omega k + u_k))$ where $u_k = \arcsin(v_k)$ and v_k is an IUD dither as before. Note that the dither here is in the phase of the *cosine* instead of the amplitude as in Fig. 4.

To reduce the output noise level introduced by the dither, at least in the vicinity of the carrier frequency Ω, one can consider estimating the phase error of the quantized output x_k, with $\cos(\Omega k)$ as the reference, and feeding it back in the form of δ_k as shown in Fig. 13.

Setting $\varepsilon_k \triangleq u_k + \delta_k$ we write the phase as $\theta_k = \Omega k + \varepsilon_k$. Expressing the output x_k as a Fourier series gives [25]

$$x_k = \frac{4}{\pi}\sum_{n=0}^{\infty}\frac{(-1)^n}{2n+1}\cos\left((2n+1)\Omega k + (2n+1)\varepsilon_k\right) \quad (15)$$

with the fundamental harmonic term being $\cos(\Omega k + \varepsilon_k)$. Multiplying the last one by $\sin(\Omega k)$ gives

$$\sin(\Omega k)\cos(\Omega k + \varepsilon_k) = -\frac{1}{2}\sin(\varepsilon_k) + \frac{1}{2}\sin(2\Omega k + \varepsilon_k). \quad (16)$$

To illustrate the architecture we make some simplifying assumptions: Feedback δ_k is such that the phase deviation ε_k is small and with low frequency content; and, the higher harmonics $(n = 1, 2, 3, \ldots)$ have small amplitude or are far in frequency from the fundamental. Note that u_k here (Fig. 13) can be small and low-pass by construction (in contrast to u_k in Fig. 12). Based on these assumptions $\sin(\varepsilon_k) \cong \varepsilon_k$ and

$$\sin(\Omega k)x_k \cong -\frac{2}{\pi}\varepsilon_k + \text{Higher Frequency Terms}. \quad (17)$$

Therefore, we can extract ε_k by low-pass filtering $\sin(\Omega k)x_k$. The complete operation is captured in Fig. 14 where $F(z)$ is a low-pass filter.

Based on the simplifying assumptions, an approximate linear phase-domain model of the phase error ε_k is shown in Fig. 15 We conclude that the dithering-to-output-phase noise transfer function is

$$\mathrm{NTF}(z) \triangleq \frac{E(z)}{U(z)} = \frac{\pi}{\pi + 2KF(z)}. \quad (18)$$

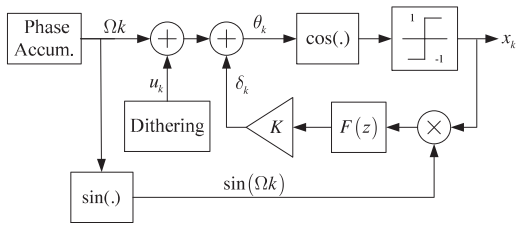

Fig. 14. Phase-domain Σ–Δ modulation scheme.

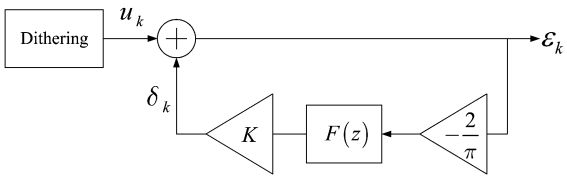

Fig. 15. Approximate linear model of the phase error ε_k.

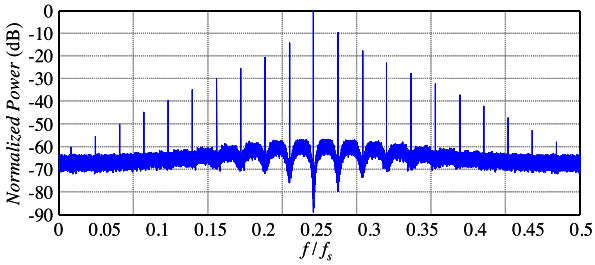

Fig. 16. Spectrum of the phase-domain Σ–Δ single-bit frequency synthesizer. Parameters: $w = 8001$, $n = 15$, clock is $f_s = 1$ GHz, averaging is set to 14 frames and resolution bandwidth is 3391 Hz.

Then the PSD of ε_k which approximately captures the residual phase noise of the output is given by $S_\varepsilon(\omega) = |\mathrm{NTF}(e^{j\omega})|^2 S_u(\omega)$. It can be useful to select $F(z)$ such that $|F(e^{j\omega})| \to \infty$ as $\omega \to 0$ so that we also get $S_\varepsilon(\omega) \to 0$. Using an integrator as a filter, i.e. $F(z) = z^{-1}/(1 - z^{-1})$, so that the loop in Fig. 15 resembles a standard first-order Σ–Δ modulator, we get that

$$S_\varepsilon(\omega) = \frac{2\pi^2\,(1-\cos(\omega))}{\pi^2+(2K-\pi)^2+2\pi(2K-\pi)\cos(\omega)} S_u(\omega) \quad (19)$$

and the resulting spectrum is illustrated in the example below.

Stability: For the modulator loop to be meaningful it has to be stable. If one considers given the fixed filter $F(z)$ then one can derive the interval(s) of the gain coefficient K for which the loop is stable. Root locus techniques and the Nyquist diagram can be helpful [22].

Example: For $\Omega = 2\pi w/2^n$ with $w = 8001$, $n = 15$, $K = 0.05$ and using low-pass dithering, the output spectrum is shown in Fig. 16 whereas the spectrum of $\mathrm{sgn}(\cos(\Omega k))$ is shown in Fig. 17 for comparison.

Figs. 18 and 19 are zoom-in versions of Figs. 16 and 17 respectively demonstrating the near-in spectrum. In Fig. 18 the dashed white line is the estimated near-in noise based on (19). Note that the spectrum in Fig. 18 is estimated with RBW of 223 Hz and so the near-in DR is in principle 23.5 dB higher than shown in the figure, i.e., about 118.5 dBc/Hz. The clarity

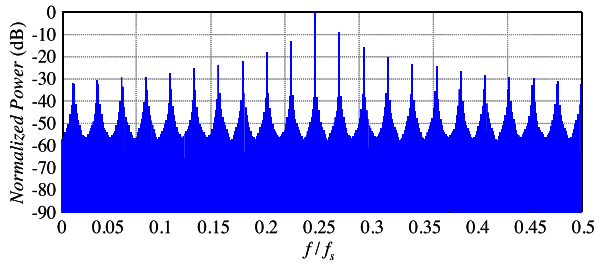

Fig. 17. Spectrum of undithered PDDS with $w = 8001$, $n = 15$.

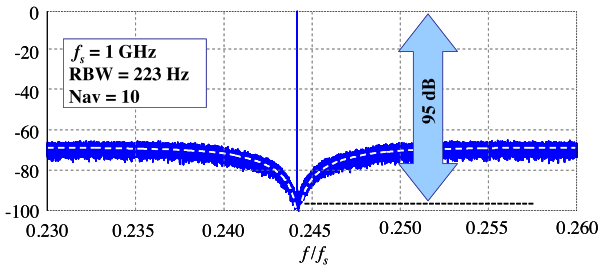

Fig. 18. Zoom-in of Fig. 16.

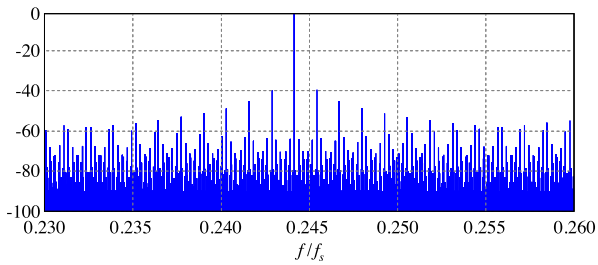

Fig. 19. Zoom-in of Fig. 17.

of the near-in spectrum however should be verified further with simulation as spurs may be hidden under the noise floor.

The advantage of the phase-domain Σ–Δ modulator in Fig. 14 is its low computational requirements. Especially in the case that no dither is used and the simple integrator is used as the loop filter, the structure is essentially multiplier-less since the multiplication is only with ±1. Moreover, the cosine LUT is not needed in practice as the output is only the sign of it.

On the other hand the disadvantage of this architecture is that it cannot control the amplitude of the cosine component of the output signal. This results in large spurs away from the carrier.

B. Polar Σ–Δ Modulation

To bypass the limitations of the phase-domain Σ–Δ modulator for single-bit output synthesis, we introduce the concept of *polar* Σ–Δ modulation. Here, in addition to feeding back the estimated phase error we do the same for the amplitude error as well. A legitimate question of course is how we can control the amplitude of a binary ±1 signal. The answer is given in the following subsection.

1) Amplitude Control of Binary Quantized Sinewave: Although we cannot control the instantaneous amplitude of the

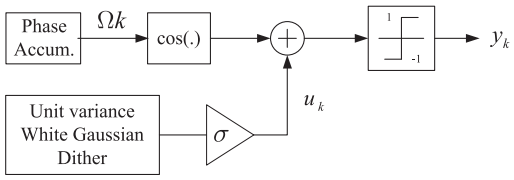

Fig. 20. Amplitude control of ± 1 sinewave-like signals.

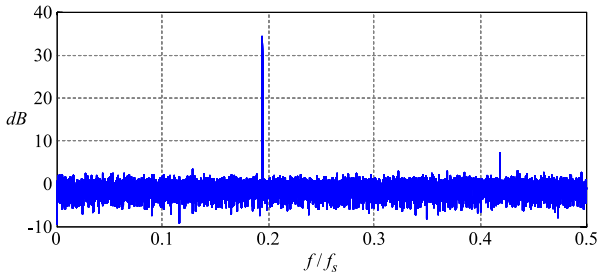

Fig. 21. Typical output spectrum of the scheme in Fig. 20.

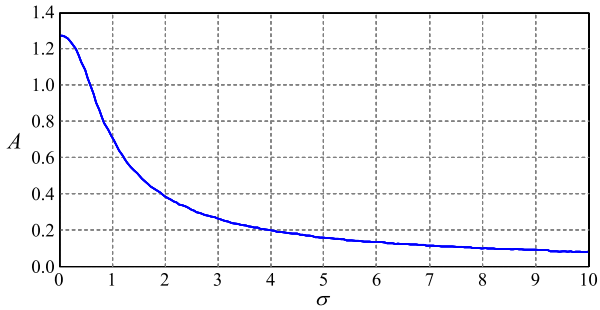

Fig. 22. Amplitude of the fundamental sinusoidal component at the output of the scheme in Fig. 20 as a function of dither's standard deviation σ.

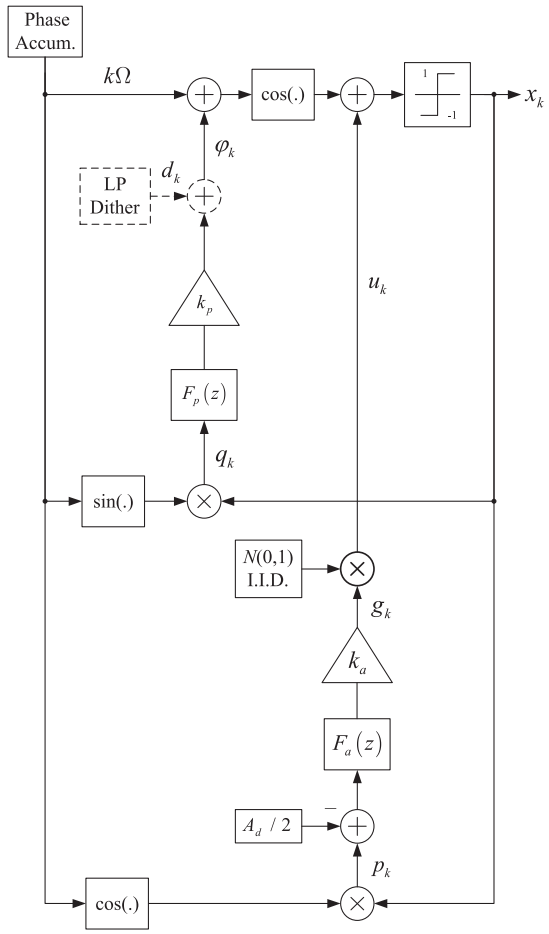

Fig. 23. Introduced polar Σ–Δ modulation architecture for single-bit output all-digital frequency synthesis.

± 1 quantized sinewave, we can do so for the amplitude of the sinewave component of it. One way of doing this indirectly is by introducing an additive noise to the cosine sequence. The concept is illustrated in Fig. 20.

Here $y_k = \mathrm{sgn}(\cos(\Omega k) + u_k)$ where u_k is a zero-mean, white Gaussian random sequence of variance σ^2. The structure is similar to the dithered PDDS in Fig. 2 but here we use Gaussian rather than uniformly distributed white noise. As expected, the spectrum of y_k contains a noise component and in most cases spurs as well, as shown in Fig. 21.

It can be shown that the output can be expressed as $y_k = A\cos(\Omega k) + n_k +$ Harmonics, where harmonics higher than a certain index are aliased and n_k is the noise component. Also, the cosine amplitude A is the following function of σ

$$A(\sigma) = \sqrt{\frac{2}{\pi}} \cdot \frac{1}{\sigma} \cdot M\left(\frac{1}{2}, 2, -\frac{1}{2\sigma^2}\right). \tag{20}$$

where $M(a, b, z)$ is Kummer's confluent hypergeometric function which can be expressed as [25], [26]

$$M(a, b, z) = \sum_{n=0}^{\infty} \frac{a(a+1), \ldots, (a+n-1)}{b(b+1), \ldots, (b+n-1)} \cdot \frac{z^n}{n!}.$$

The graph of (20) is shown in Fig. 22.

2) Polar Σ–Δ Modulation Single-Bit-Output Synthesizer: The proposed polar Σ–Δ modulation scheme is shown in Fig. 23. To illustrate its operation we express the output of the quantizer as $x_k = A_k \cos(\Omega k + \varphi_k) + n_k$. Random sequences A_k and φ_k are considered such that $A_k \cos(\Omega k + \varphi_k)$ equals the sum of the carrier and the noise and spurs with frequency offset less than the bandwidth of *low-pass* filters F_p and F_a from the carrier (assume for simplicity that they have the same bandwidth). Also, n_k represents the remaining noise and spurs with offset frequencies from the carrier larger than the bandwidth of the filters.

Then $p_k = (A_k/2)\cos(\varphi_k) + (A_k/2)\cos(2k\Omega + \varphi_k) + \eta_k$ (Fig. 23) where the term $\eta_k = \cos(k\Omega)n_k$ has frequency content only outside of the bandwidth of F_a. Assume that $|\varphi_k|$ is sufficiently small, i.e. $\cos(\varphi_k) \cong 1$, and that Ω is sufficiently smaller than π, to prevent the second harmonic and the spectrum of η_k from being aliased near zero. Then, $g_k \cong (k_a/2)(f_a \otimes (A_k - A_d))_k + \xi_k$ where A_d is the desirable amplitude and ξ_k is the remaining low-frequency noise. The standard deviation of the dither u_k equals g_k (Fig. 23) and so the amplitude of the output cosine component A_k is a decreasing function of g_k following (20) (and Fig. 22). This completes the amplitude control loop.

Similarly, from Fig. 23 we get that for the phase control loop $q_k \cong -(A_k/2)\sin(\varphi_k) + (A_k/2)\sin(2k\Omega + \varphi_k) + \tilde{\eta}_k$ where

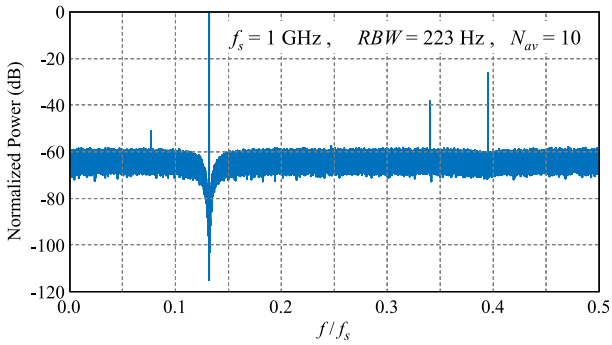

Fig. 24. Polar modulator's output spectrum following Example 1. Clock frequency f_s is set to 1 GHz, averaging is set to 10 frames and resolution bandwidth is 223 Hz.

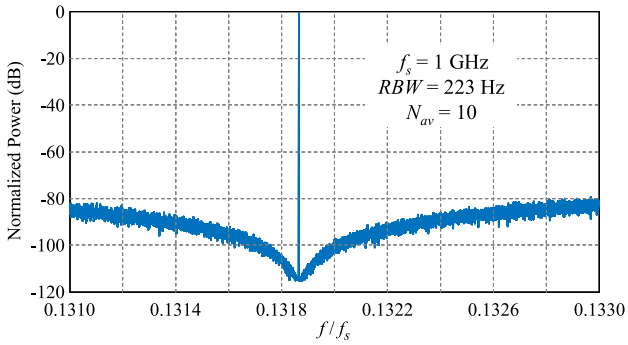

Fig. 25. Near-in zoom in of Fig. 24.

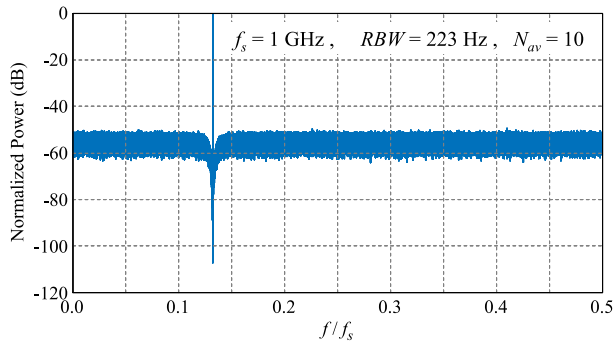

Fig. 26. Polar modulator's output spectrum following Example 1, but with desirable amplitude set to $A_d = 0.5$.

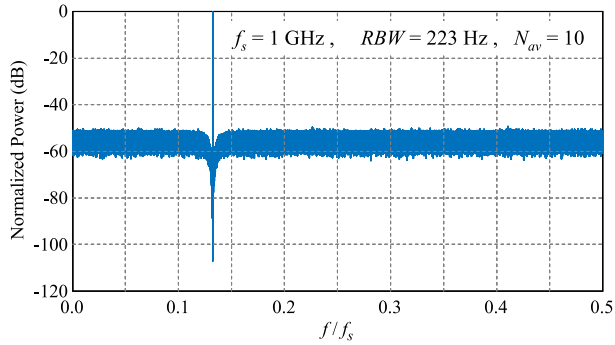

Fig. 27. Polar modulator's output spectrum following Example 2. Clock frequency f_s is set to 1 GHz, averaging is set to 10 frames and resolution bandwidth is 223 Hz.

$\tilde{\eta}_k = \sin(k\Omega)n_k$. Using the same reasoning as above, as well as making the approximation $\sin(\varphi_k) \cong \varphi_k$, we conclude that $\varphi_k \cong -(k_p/2)(f_p \otimes (A_k\varphi_k))_k + d_k + \tilde{\xi}_k$ where $\tilde{\xi}_k$ is the remaining low-frequency noise and d_k is the optional dither.

Note that $(f_p \otimes (A_k\varphi_k))_k$ is a bilinear functional on $\{A_k\}$ and $\{\varphi_k\}$. If one further assumes that $\{A_k\}$ has significantly lower bandwidth than f_p then we can make the additional approximation that $\varphi_k \cong -(k_pA_k/2)(f_p \otimes (\varphi_k))_k + d_k + \tilde{\xi}_k$.

The following examples illustrate the behavior of the polar Σ–Δ modulator.

Example 1: Consider the first-order Σ–Δ equivalent with $F_a(z) = F_p(z) = z^{-1}/(1 - z^{-1})$ (here we have two coupled first-order loops). Gain coefficients are set to $k_p = 1/8$ and $k_a = 1/4$. The desirable output amplitude is set to $A_d = 1$ and the phase low-pass dither is deactivated. Finally, the carrier frequency is set to $\Omega = 2\pi(4321/32768)$.

The output spectrum is shown in Fig. 24. The two spurs on the right are the 3rd and 5th harmonics. They are partially due to the strong nonlinearity of the amplitude function (20) near zero σ, since the desirable amplitude level has been set to the large value $A_d = 1$. Fig. 24 should be compared to Fig. 26 where smaller desirable amplitude, $A_d = 0.5$, is set.

A zoom-in near the carrier shown in Fig. 25 indicates a bandpass Σ–Δ like behavior [2], [22], [27]. Even though phase dithering is not used, there are no apparent spurs.

Changing the desirable amplitude to $A_d = 0.5$ the spurs in Fig. 24 disappear as it is seen in Fig. 26. Also, the noise floor is raised about 3 dB—with respect to the carrier (note that the spectra are normalized to the carrier power).

Example 2: Consider again the first-order Σ–Δ equivalent with $F_a(z) = F_p(z) = z^{-1}/(1 - z^{-1})$. Gain coefficients now are set to $k_p = 1/8$ and $k_a = 3/8$. The desirable output amplitude is set to $A_d = 0.5$ and the phase low-pass dither is deactivated. Finally, it is $\Omega = 2\pi(4321/32768)$ as before.

Lower desirable amplitude A_d and stronger amplitude feedback k_a, with respect to Example 1, have eliminated spurs as shown in Fig. 27 (compared to Fig. 24) and raised the noise floor, similarly to Fig. 26. A zoom-in illustrates similar bandpass Σ–Δ like behavior as in Example 1, Fig. 28.

Example 3: Consider now the polar modulator with amplitude transfer function

$$F_a(z) = \frac{z^{-1}}{1 - z^{-1}} \cdot \frac{(1 - r_z e^{j\Omega_z} z^{-1})(1 - r_z e^{-j\Omega_z} z^{-1})}{(1 - e^{j\Omega_p} z^{-1})(1 - e^{-j\Omega_p} z^{-1})},$$

phase transfer function $F_p(z) = z^{-1}F_a(z)$, $\Omega_z = 5.5 \cdot 10^{-4} \cdot 2\pi$, $r_z = 0.99$ and $\Omega_p = 5 \cdot 10^{-4} \cdot 2\pi$.

Fig. 29 illustrates the placement of poles and zeros of the transfer functions. The gain coefficients are set to $k_a = k_p = 1/8$ and the desirable output amplitude is $A_d = 0.9$. Again, the phase low-pass dither is deactivated and the carrier frequency is set to $\Omega = 2\pi(4321/32768)$ as before.

The output spectrum is shown in Fig. 30 and a zoom-in near the carrier is shown in Fig. 31, with the same scaling as that of Fig. 28 for comparison. The notch points are at the frequencies Ω and $\Omega \pm \Omega_p$. An intermediate zoom-in of Fig. 30 illustrating the second-order Σ–Δ noise shaping behavior is shown in Fig. 32.

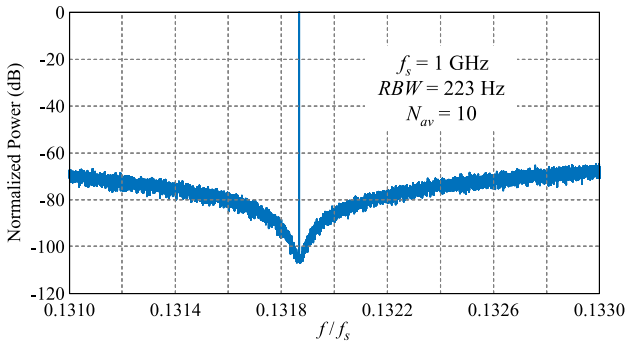

Fig. 28. Near-in zoom in of Fig. 27.

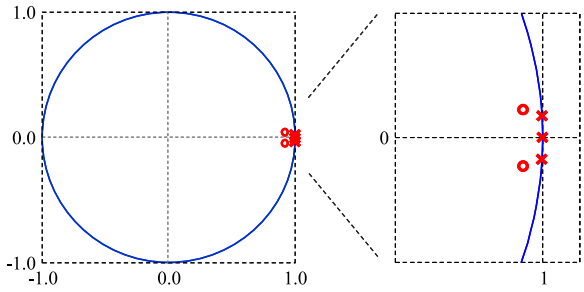

Fig. 29. Poles and zeros of the transfer function $F_a(z)$.

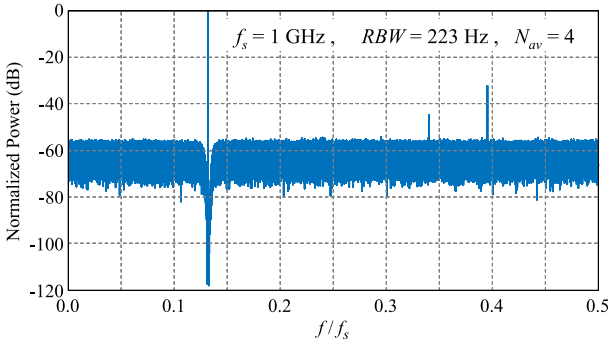

Fig. 30. Polar modulator's output spectrum following Example 3. Clock frequency f_s is set to 1 GHz, averaging is set to 4 frames and resolution bandwidth is 223 Hz.

C. Comments on Phase and Polar Feedback Architectures

Both the phase and polar Σ–Δ architectures introduced are capable of noise shaping and spurs elimination in the near-in spectrum. Phase Σ–Δ has low computational complexity but its output contains strong spurs away from the carrier. On the other hand polar Σ–Δ architecture can eliminate (or at least suppress) spurs throughout the whole spectrum at the extra cost of a multiplier and a *sine* LUT.

IV. Conclusion

Two classes of single-bit output all-digital frequency synthesis architectures were discussed characterized by their spurs and noise reduction mechanism: The loop-less *forward* one with direct dithering for spurs elimination, which offers simplicity and broadband spurs-free output but converts all dither power to noise floor; and two *feedback* architectures, the *phase* Σ–Δ and

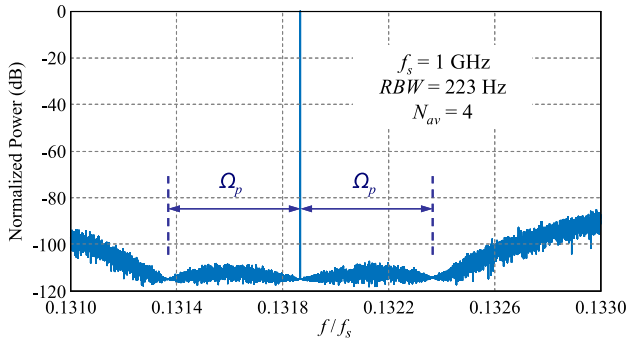

Fig. 31. Near-in zoom in of Fig. 30.

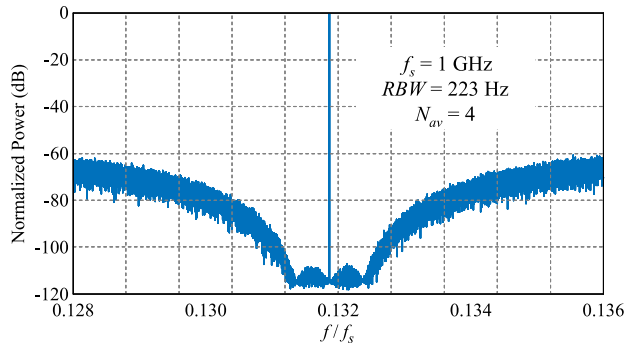

Fig. 32. Zoom-in of Fig. 30 illustrating second-order Σ–Δ noise shaping behavior.

the *polar* Σ–Δ, both introduced here, which offer high dynamic range near-in with a noise-shaping and spurs-eliminating behavior similar to classical band-pass Σ–Δ. The *phase* architecture is multiplier-less offering simplicity and low computational complexity but its output may contain strong spurs away from the carrier. The *polar* architecture offers better near-in noise and spurs suppression as well as spurs suppression throughout the whole spectrum at the cost of an extra multiplier and a sine LUT. Both the phase and polar architectures introduced here are nonlinear dynamical systems more involved mathematically than the standard Σ–Δ modulator. Further analysis of their operation is important as well as practical implementations of them.

References

[1] W. Kester, Ed., *Data Conversion Handbook (Analog Devices)*. Burlington, MA, USA: Newnes, 2005.
[2] J. Vankka and K. Halonen, *Direct Digital Synthesizers: Theory, Design and Applications*. New York, NY, USA: Springer, 2006.
[3] C. E. Wheatley, III, "Digital frequency synthesizer with random jittering for reducing discrete spectral spurs," Patent 4410954, 1983.
[4] V. S. Reinhardt, "Direct digital synthesizers," Hughes Aircraft Co, Space and Comm. Group, CA Tech. Rep., Dec. 1985.
[5] V. N. Kochemasov and A. N. Fadeev, "Digital-computer synthesizers of two-level signals with phase-error compensation," *Telecommun. Radio Eng.*, vol. 36/37, pp. 55–59, Oct. 1982.
[6] R. Staszewski and P. Balsara, *All-Digital Frequency Synthesizer in Deep-Submicron CMOS*. Hoboken, NJ, USA: Wiley, 2006.
[7] E. Temporiti, C. Weltin-Wu, D. Baldi, R. Tonietto, and F. Svelto, "A 3 GHz fractional all-digital PLL with a 1.8 MHz bandwidth implementing spur reduction techniques," *IEEE J. Solid-State Circuits*, vol. 44, no. 3, pp. 824–834, Mar. 2009.
[8] P. Sotiriadis and K. Galanopoulos, "Direct all-digital frequency synthesis techniques, spurs suppression and deterministic jitter correction," *IEEE Trans. Circuits Syst. I, Reg. Papers*, vol. 59, no. 5, pp. 958–968, May 2012.

[9] K. Galanopoulos and P. Sotiriadis, "Optimal dithering sequences for spurs suppression in pulse direct digital synthesizers," in *Proc. IEEE Int. Freq. Control Symp. (FCS)*, 2012, pp. 1–4.
[10] P. Sotiriadis, "Spectral properties of dithered nyquist-rate single-bit quantized amplitude-modulated sinewaves," in *Proc. IEEE Int. Freq. Control Symp. (FCS)*, 2014, pp. 1–5.
[11] P. Sotiriadis, "All digital frequency synthesis based on pulse direct digital synthesizer with spurs free output and improved noise floor," in *Proc. IEEE Int. Freq. Control Symp. (FCS)*, 2014, pp. 1–5.
[12] U. L. Rohde, *Microwave and Wireless Synthesizers: Theory and Design*, 1st ed. Singapore: Wiley-Interscience, 1997.
[13] L. Ljung, *System Identification: Theory for the User*, 2nd ed. Upper Saddle River, NJ, USA: Prentice-Hall, 1999.
[14] P. Sotiriadis, "On the generation of random dithering sequences with specified both power spectral density and probability density function," in *Proc, IEEE Int. Freq. Control Symp.*, 2014, pp. 1–5.
[15] H. Mair and L. Xiu, "An architecture of high-performance frequency and phase synthesis," *IEEE J. Solid-State Circuits*, vol. 35, no. 6, pp. 835–846, Jun. 2000.
[16] H. Mair, L. Xiu, and S. A. Fahrenbruch, "Precision frequency and phase synthesis," Patent 6 329 850 B1, Dec. 11, 2001.
[17] L. Xiu and Z. You, "A "flying-adder" frequency synthesis architecture of reducing VCO stages," *IEEE Trans. Very Large Scale Integr. (VLSI) Syst.*, vol. 13, no. 2, pp. 201–210, Feb. 2005.
[18] D. E. Calbaza and Y. Savaria, "A direct digital periodic synthesis circuit," *IEEE J. Solid-State Circuits*, vol. 37, no. 8, pp. 1039–1045, 2002.
[19] P. Sotiriadis, "Theory of flying-adder frequency synthesizers part I: Modeling, signals periods and output average frequency," *IEEE Trans. Circuits Syst. I, Reg. Papers*, vol. 57, no. 8, pp. 1935–1948, Aug. 2010.
[20] P. Sotiriadis, "Theory of flying-adder frequency synthesizers part II: Time and frequency domain properties of the output signal," *IEEE Trans. Circuits Syst. I, Reg. Papers*, vol. 57, no. 8, pp. 1949–1963, Aug. 2010.
[21] P. Sotiriadis, "Exact spectrum and time-domain output of flying-adder frequency synthesizers," *IEEE Trans. Ultrasonics, Ferr., Freq. Control*, vol. 57, no. 9, pp. 1926–1935, Sep. 2010.
[22] R. Schreier and G. C. Temes, *Understanding Delta-Sigma Data Converters*. Piscataway, NJ, USA: IEEE Press–Wiley Intercience, 2005.
[23] G. I. Bourdopoulos, A. Pnevmatikakis, V. Anastassopoulos, and T. L. Deliyannis, *D. S. Modulators: Modeling, Design and Applications*. London, U.K: Imperial College Press, 2003.
[24] J. Vankka, *Digital Synthesizers and Transmitters for Software Radio*. Dordrecht, The Netherlands: Springer, 2005.
[25] M. Abramowitz and I. A. Stegun, Eds., *Handbook of Mathematical Functions: with Formulas, Graphs, Mathematical Tables* ser. Dover Books on Mathematics. New York, NY, USA: Dover, 1965.
[26] A. Gelb and W. E. Vander Velde, *Multiple-Input Describing Functions and Nonlinear Systems Design* ser. Electronic Sciences Series. New York, NY, USA: McGraw-Hill.
[27] S. A. Jantzi, K. W. Martin, and A. S. Sedra, "Quadrature bandpass Σ/Δ modulation for digital radio," *IEEE J. Solid State Circuits*, vol. 32, no. 12, pp. 1935–1950, Dec. 1997.

Paul P. Sotiriadis (SM'09) received the Diploma degree in electrical and computer engineering from the National Technical University of Athens, Greece, the M.S. degree in electrical engineering from Stanford University, Stanford, CA, USA, and the Ph.D. degree in electrical engineering and computer science from the Massachusetts Institute of Technology, Cambridge, MA, USA, in 2002. In 2002, he joined the Johns Hopkins University, Baltimore, MD, USA, as Assistant Professor of Electrical and Computer Engineering. In 2012, he joined the faculty of the Electrical and Computer Engineering Department of the National Technical University of Athens, Greece. He has authored and coauthored more than 90 technical papers in IEEE journals and conferences, holds one patent, has several patents pending, and has contributed chapters to technical books. His research interests include design, optimization, and mathematical modeling of analog and mixed-signal circuits, RF and microwave circuits, advanced frequency synthesis, biomedical instrumentation, and interconnect networks in deep-submicrometer technologies. He has led several projects in these fields funded by U.S. organizations and has collaborations with industry and national labs. He has received several awards, including a Best Paper Award in the IEEE International Symposium on Circuits and Systems 2007, a Best Paper Award in the IEEE International Frequency Control Symposium 2012 and the 2012 Guillemin-Cauer Award from the IEEE Circuits and Systems Society. Dr. Sotiriadis is an Associate Editor of the IEEE TRANSACTIONS ON CIRCUITS AND SYSTEMS—PART I: REGULAR PAPERS and the IEEE Sensors Journal, has served as an Associate Editor of the IEEE TRANSACTIONS ON CIRCUITS AND SYSTEMS—PART II: EXPRESS BRIEFS from 2005 to 2010 and has been a member of technical committees of many conferences. He regularly reviews for many IEEE transactions and conferences and serves on proposal review panels.